Ultraviolet astronomy with the International Ultraviolet Explorer

P. M. Gondhalekar* S R C, Rutherford & Appleton Laboratory,
Chilton, Didcot, Oxon

Abstract. Astronomical research with the International Ultraviolet Explorer has been reviewed.

Key words : ultraviolet astronomy — IUF

1. Introduction

The strong attenuation by the terristrial atmosphere at wavelengths shorter than 3200 Å and the attenuation at the Lyman limit (912 Å) by interstellar hydrogen provide a natural definition of the "ultraviolet (UV) spectral region". In this review, the results of spectrophotometric observations in the 912–3200 Å region have been described. The importance of astronomical observations at ultraviolet wavelengths has been recognized since the rocket-initiated era of space research. Apart from the large extension of the observed spectrum, the presence in the UV region of the resonance lines of the most abundant molecular and atomic/ionic species is a strong justification for astronomical observations at these wavelengths. The pioneering observations in UV astronomy were made with unstabilized rocket payloads which scanned the sky with simple photometric systems by the free motion of the vehicles (Kupperian *et al.* 1958). Because of the short observing time per object permitted by unstabilized rockets, only very coarse spectral resolution was possible even for a bright star. The full development of the UV rocket astronomy was attained with stabilized payloads, and resolutions of ∼1 Å was achieved (Morton & Spitzer 1967). More systematic sky scans and greater observing time per object can be achieved with comparatively simple satellites furnished with some degree of control for scan rate or scan direction (Smith 1967; Kurt & Syunyaev 1968). Space observatories were possible with the development of stabilized satellite platforms. An observatory satellite consists of two parts, the spacecraft and the scientific instruments. The spacecraft provides power, data storage, communication facility, timing and command signals; it also has orientation capability and to a large degree defines the thermal environment of the scientific payload. The first successful satellite observatory was launched

*Present address : E S A, Villafranca del Castellio Satellite Tracking Station, P.O. Box 54065, Madrid, Spain.

in 1968 December (OAO-A2) with payloads prepared by the Smithsonian Astrophysical Observatory (the Celescope project) and the University of Wisconsin. Since then, a number of satellite observatories have been launched which have scientific packages of varying sophistication and are capable of high photometric accuracy and high spectroscopic resolution. The characteristics of the scientific instruments on these observatory satellites are given in Table 1 and Figure 1. A new era in space astronomy has been started with the launching of International Ultraviolet Explorer (IUE). An astronomer can now plan and execute his observing program and view his data in real-time as he would at a ground based observatory. In this review, the ultraviolet data obtained with IUE are discussed; this review is not exhaustive and only the highlights of astrophysical research are described. In section 2, the IUE spacecraft, the IUE scientific instrument, and the operation of an "IUE Observatory" are described. In the following seven sub-sections, the IUE observations of solar system objects, cool stars (spectral type A—M), hot stars (spectral types dO – B), interstellar medium (galactic), high energy objects (*e.g.* x-ray binaries), normal

Table 1. Orbiting astronomical observatories

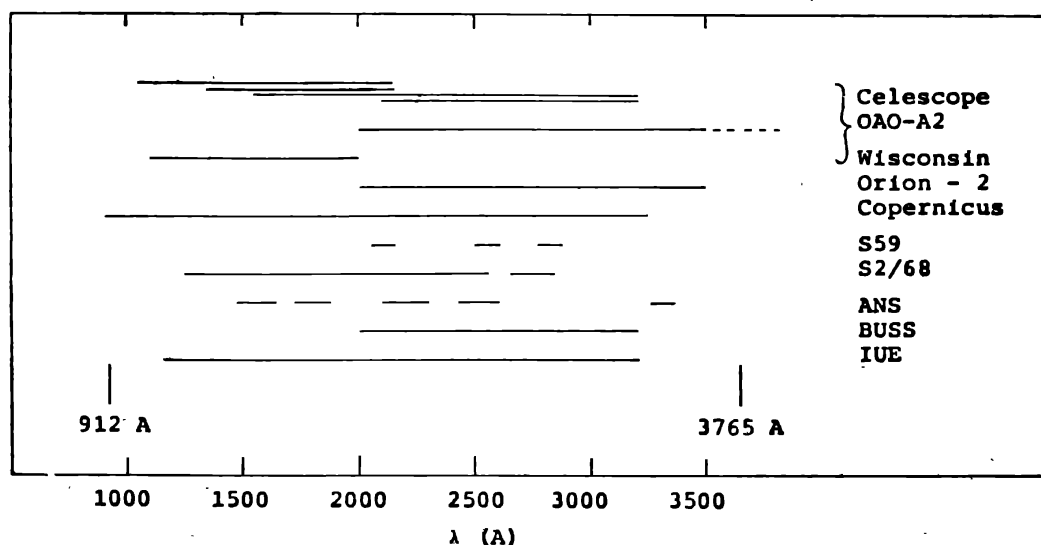| Name	Telescope	Mode	Resolution	Limiting m_V
OAO-A2	30 cm			12
Celescope		Photometric		
Wisconsin		Spectroscopic	10-200 Å	
Copernicus	80 cm	Spectroscopic	0.05-0.1 Å	6
Orion-2*	24 cm	Spectroscopic	8-28 Å	12-13
S59	22 cm	Spectroscopic	1.8 Å	10
S2/68	27.5 cm	Spectroscopic	35 Å	12
BUSS	40 cm	Spectroscopic	0.1 Å	6
IUE	45 cm	Spectroscopic	0.1-0.2 Å	12
			6-8 Å	17

*Gurzadyan 1975

Figure 1. Wavelength coverage of ultraviolet satellite observatories.

galaxies, and active galaxies have been described. A detailed description of the IUE, its post-launch performance, and the data obtained during the commissioning phase following the successful launching in 1978 January are described in a special issue of *Nature* (Volume 275, 1978 October 5).

2. International Ultraviolet Explorer

2.1. THE SPACECRAFT

An "exploded" view of the IUE spacecraft is shown in Figure 2, and the spacecraft characteristics are given in Table 2. The main body of the spacecraft is octagonal in shape, the telescope protruding from one end and the apogee boost motor from the opposite end. Two solar arrays extend from two opposite sides of the octagon, and when in orbit, the spacecraft is oriented around the telescope axis to keep the array-face towards the Sun. The apogee boost motor is used to inject the spacecraft into a synchronous orbit, and the hydrazin auxiliary propulsion system is used to manoeuvre the spacecraft. An approximate altitude is maintained by six inertial-grade gyroscopes and a two axis solar sensors. The spacecraft in orbit can be mano-euvred by a set of momentum exchange reaction wheels, which rely on hydrazin thrusters for momentum exchange.

The telescope and two spectrographs are rigidly connected together and are attached to the central strong ring of the spacecraft. The inertial reference system is attached to the scientific instrument and an off-set star tracker within the scientific instrument provides an absolute reference frame from the coordinates of a celestial target. The off-set tracker also provides reference signals to correct the drift of the spacecraft and the pointing accuracy is about 0.1 arcsec.

2.2. THE SCIENTIFIC INSTRUMENT

The scientific instrument consists of a telescope, two fine error sensors, two echelle spectrographs and four SEC cameras. The 45-cm f/15 Cassegrain telescope has a Ritchey-Chrétien figure and produces a uniform image over a 16 arcmin field of view. The primary is made of beryllium and the secondary of fused silica. The telescope tube is made of aluminium and wrapped in aluminized Mylar thermal insulation The telescope sunshade is cut at 43° with respect to the optic axis of the telescope, which can be pointed anywhere in the sky at an angle greater than 43° to the Sun. The sunshade and the telescope tube are baffled to prevent scattered

Table 2. IUE spacecraft characteristics

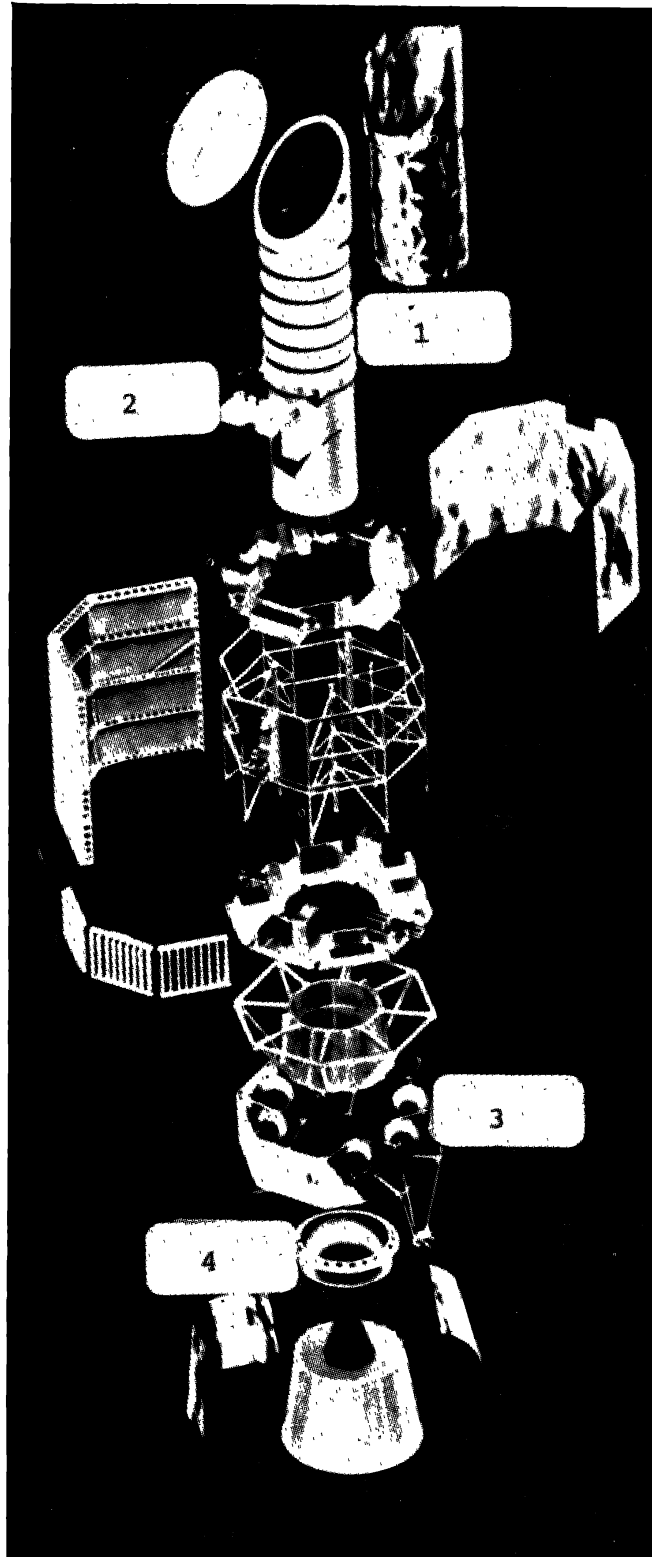|	
Weight	636 kg
Height	421 cm
Life	3–5 yr
Stability	<1 arcsec
Orbit	elliptical
	geosynchronous
Inclination	28.6°
Apogee	45887 km
Perigee	25669 km
Eccentricity	0.24

Figure 2. An "exploded" view of IUE scientific instrument; (1) telescope tube and sunshade, (2) gyroscopes, (3) hydrazin auxiliary propulsion system, (4) apogee boost motor.

light from reaching the primary mirror. The aperture plate for the spectrographs is mounted in the focal plane of the telescope behind the primary and is tilted at 45° to the telescope axis. The aperture plate reflects the telescope field into a fine Error Sensor (FES). Two FESs (primary and redundant) serve the dual purpose of off-set star tracker and field camera. A FES scans the 16 arc min field of view of the telescope, and an image of this field is transmitted to an observatory for identification by an astronomer. After an astronomical target has been moved to an entrance aperture of a selected spectrograph (by manoeuvring the spacecraft), the FES can be off-set to any other star in the field of view to generate error signals to hold the spacecraft on target. The limiting magnitude of the FES depends on its mode of operation, but a FES can track on stars as faint as 12 mag. The spectral response of a FES is between visible and blue, and the FES counts can be converted to visual magnitudes by the following relations:

$$m_{FES} = -2.5 \log C + 16.58, \qquad \text{mode : fast/overlap}$$
$$= -2.5 \log C + 11.05, \qquad \text{fast/underlap}$$
$$= -2.5 \log C/4 + 16.58, \qquad \text{slow/overlap}$$
$$m_v = m_{FES} - 0.24 (B - V),$$

where C is the total number of FES counts.

Behind the aperture plate, there are two spectrographs, which cover the spectral ranges 1150–2000 Å and 1900–3200 Å, respectively. Each spectrograph has a pair of entrance apertures consisting of a 3 arcsec circular hole and a 10 ×20 arcsec approximately-elliptical slot. Any particular aperture can be selected by pointing the telescope so that the target image lies in the required aperture. The two large apertures can be closed but the small apertures stay open.

In their optical configuration the two spectrographs are identical; light from a target passes through an entrance aperture and is collimated by an off-axis paraboloid. The collimated beam is incident on an echelle grating and is defracted to a spherical concave grating which separates the echelle orders and focuses the image of the entrance aperture on the face-plate of a camera detector. A plane mirror can be inserted in front of the echelle grating to obtain a low dispersion spectrum produced by the concave grating. The short wavelength spectrograph is on the optic axis of the telescope whereas the long wavelength spectrograph is off-set from it. Light from the telescope is input to this spectrograph by two plane mirrors inclined at 45°. All optical surfaces in the two spectrographs are front aluminized but the 45° deflection mirrors and the collimator of the long wavelength spectrograph are overcoated with silicon oxide to suppress the second order spectrum. The rest of the optical surfaces are overcoated with magnesium fluoride.

A spectrum is detected by a television camera. There are two cameras in each spectrograph (a primary and a redundant unit) and all cameras are identical in construction. A camera integrates a two-dimensional image during an exposure and converts the image into video signals suitable for transmission to ground control. The basic detector unit is a Ultraviolet-to-Visible Converter (UVC) coupled to a Secondary Electron Conduction (SEC) television camera sensitive only to blue light. The proximity focus UVC has a magnesium fluoride face-plate transparent to radiation above 1150 Å, and cesium telluride photocathode with a quantum efficiency of 10–15 per cent between

1150 Å and 3000 Å. The quantum efficiency drops to 0.1 per cent in the visible. A high electric field in the UVC accelerates the photoelectrons onto a phosphore screen, where the photoelectrons produce photons, whose energy is peaked in the blue. Halation in the UVC is reduced by a coating of matt black aluminium on the phosphore.

The blue image from the UVC is transferred by a fibre-optic face plate to the bi-alkali photocathode of a SEC tube. The photoelectrons generated at the photocathode are accelerated and focused electrostatically on the SEC target, which consists of a low density porous layer of potassium chloride about 10 micron thick. The potassium chloride layer is supported by an aluminium oxide layer about 500 Å thick and backed by a thin aluminium signal plate. The photoelectrons produce a positive charge image, which is stored on the target. At the end of an exposure, the image is read-out by discharging the target with a pulsed beam of electrons. The electron beam is magnetically focused and deflected digitally to scan a raster of 768 × 768 pixels in 37 micron steps across an image. At each pixel, the read beam is pulsed ON to discharge the target and the output video signal is digitized into one of 256 discrete levels (DN units), and these data are transmitted to a ground observatory in real-time. The SEC target conductance is spatially non-uniform, and the focus of the READ beam is a function of the position in the raster; thus each pixel is a unique photometer, with a unique intensity transfer function.

In addition, the scientific instrument has a number of light sources; a platinum-neon hollow cathode lamp is required to provide the wavelength calibration of the two spectrographs. Tungsten lamps are used to prepare the target of a SEC camera for a new image, and mercury lamp are required to generate intensity transfer functions of cameras. The characteristics of the scientific instrument are summarized in Table 3.

Table 3. IUE scientific instrument characteristics

Telescope

Configuration	Cassegrain
Figure	Ritchey-Chrétien
Clear aperture	45 cm
Effective focal length	675 cm
Focal ratio	15
Plate scale	30.6 arcsec mm^{-1}
Field of view	16 arcmin

Spectrographs

	Long λ	Short λ
Wavelength coverage	1150–2000 Å	1900–3200 Å
Collimator radius	18.9 cm	18.9 cm
Echelle grating ruling	101.9 mm^{-1}	63.2 mm^{-1}
blaze	45.5°	48.1°
Concave grating ruling	313.0 mm^{-1}	200.0 mm^{-1}
radius	13.7 cm	13.7 cm
Resolution high	0.1 Å	0.2 Å
low	6 Å	8 Å

P. M. Gondhalekar

2.3. THE GROUND OBSERVATORY

Unlike previous astronomy satellites, IUE is operated in real-time by guest observers, but guest observers do not require a detailed knowledge of the complex spacecraft and ground systems, as the operations are conducted by selecting preprogrammed operating sequences from a computer library. A observer can plan and execute his research program in real-time, although some prepreparation is advisable. The spectra can be displayed on an Experimental Display System (EDS) at the end of an exposure, and the quality of the image can be assessed with the aid of display options built into the EDS.

The IUE TV images can be received at either of the two observatories; the observatory at NASA's Goddard Space Flight Center is in contact with the spacecraft for 24 hours a day and the observatory at the ESA Villafranca del Castellio Satellite Tracking Station is in contact with the spacecraft for 10 hours a day. The observatories correct IUE images for the non-linear response of the SEC camera and also for the absolute response of the rest of the scientific instrument. The absolute sensitivity curves currently in use for the short and the long wavelength spectrographs are shown in Figure 3 (Bohlin *et al.* 1980). A high or a low dispersion spectrum is extracted from an image, so that the spectrum provided to an astronomer is suitable for scientific analysis.

3. Scientific program

In the two years since the launching of IUE, the satellite has been used to observe a host of astronomical objects—from nearby planets to distant quasars. Some of these observations are described in the following sections.

3.1. SOLAR SYSTEM STUDIES

3.1.1. *Outer planets*

The atmospheres of outer planets are expected to be rich in organic molecules (Sagan *et al.* 1967), and the abundances in the upper stratosphere are controlled by photochemical processes and vertical diffusion (Stobel 1975). Solar UV radiation, particularly below 2000 Å, would be reflected/scattered from a thin upper region above the tropopause, and the spectrum of this reflected/scattered radiation should provide information on the constituents in these regions of planetary atmospheres. This has been established by IUE observations of Jupiter (Owen *et al.* 1980) and Saturn (Moos & Clarke 1979). The features due to acetylene and ammonia are marked in a spectrum of Jupiter shown in Figure 4. The presence of ammonia in the atmosphere of Jupiter was well known and was suspected to affect the UV spectrum in the 2000 – 2300 Å region (Greenspan & Owen 1967; Anderson *et al.* 1969) but these observations were based on broad band data. The resolution of IUE is sufficient to identify possible ammonia features in the spectrum of the Jovian atmosphere and an upper limit for $[NH_3]/[H_2] < 0.5 \times 10^{-9}$ has been obtained from these data. This low value is consistent with the interpretation that below 2000 Å the radiation is scattered from a region above the temperature minimum which confines ammonia to deeper atmosphere.

3.1.2. *Comets*

The short reaction time of the real-time observatory mode of operation of IUE was demonstrated by observations of Comet Sargent 1978m. The spectra of this comet were obtained two weeks after its discovery and before any ground based spectroscopic observation was made (Jackson *et al.* 1979; Rahe *et al.* 1980). Atomic emission lines of H I, O I, C I, S I and molecular emission bands of OH, CS, CO_2^+ NH and CO^+ were identified. The comet was observed at different helio-centric distances to determine the H and OH production rates.

Figure 3 here. Plot labeled "Short wavelength" with y-axis s^{-1} (values 10, 4, 2) and x-axis λ (Å) (1200, 1400, 1600, 1800). Plot labeled "Long wavelength" with y-axis s^{-1} (values 20, 10, 4, 2, 1, .4) and x-axis λ (Å) (2000, 2400, 2800, 3000).
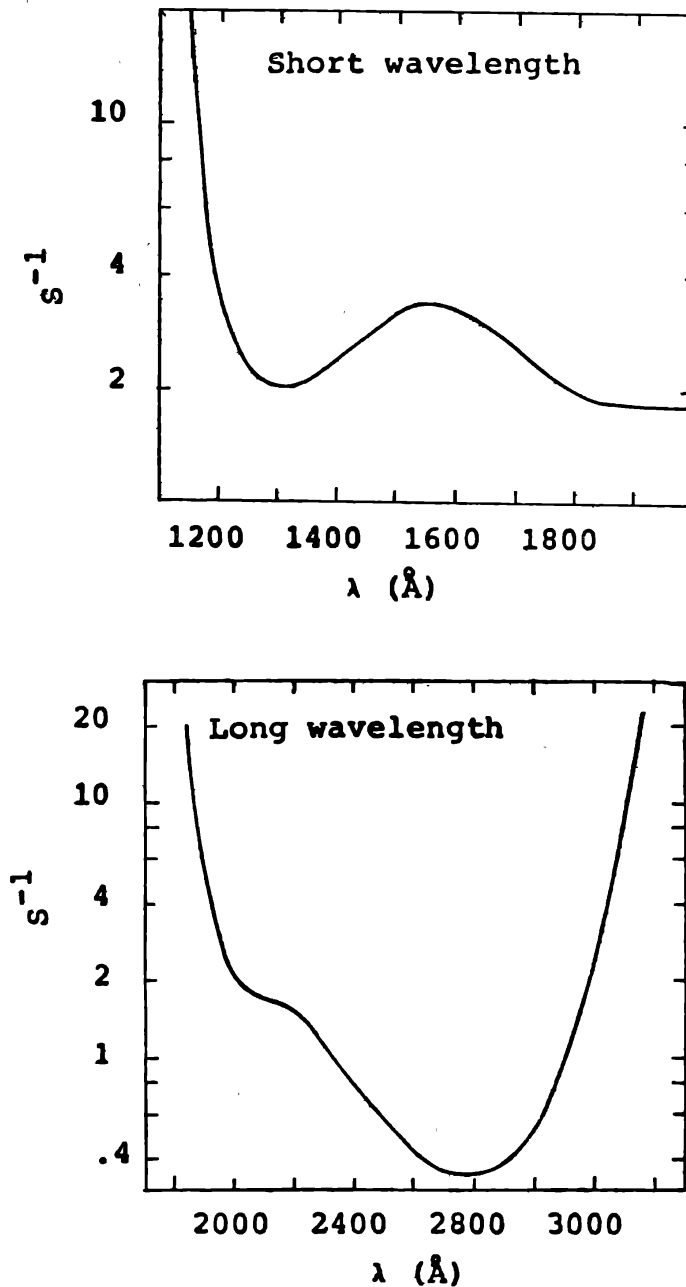
Figure 3. Absolute calibration curves for short and long wavelength spectra in low dispersion obtained through 10×20 arcsec aperture (Bohlin *et al.* 1980). S^{-1} in ergs cm^{-2} s^{-1} A^{-1} FN^{-1}.
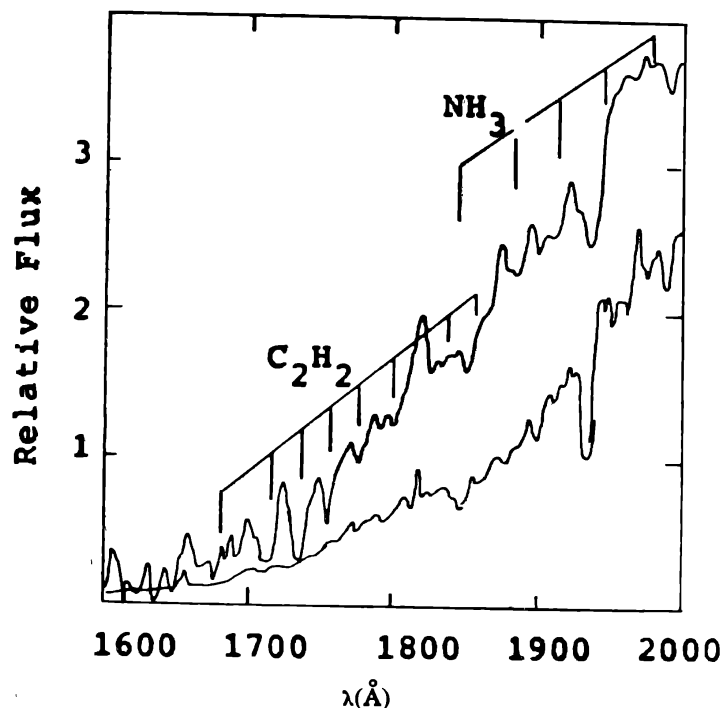
120 *P. M. Gondhalekar*

Figure 4. IUE spectra of Jupiter. An averaged solar spectrum is also shown. Positions of C_2H_2 and NH_3 absorption features are marked (Owen *et al*. 1980).

The second comet, Bradfield 1979l, was first observed with IUE on 1980 January 10 and 11 and subsequently on several occasions and at different helio-centric distances (Rahe *et al*. 1980). The atomic and molecular emissions observed in the spectrum of Comet Sargent 1978m were also detected in the spectrum of comet Bradfield 1979l and in addition, the C II (1335 Å) multiplet and the CO fourth positive bands were detected. A faint continuum near 2750 Å and 2950 Å detected in the spectrum suggests a high dust to gas ratio. This conclusion is supported by optical photometry and spectroscopy.

The main results of ultraviolet observations of comets are :

(i) detection of S I;

(ii) resolution of (0, 0) and (1, 0) bands of OH;

(iii) determination of H and OH production rates at different helio-centric distances;

(iv) determination of spatial intensity variation of CS which suggests that CS exists as a parent molecule in the cometry ice;

(v) determination of OH fluorescence efficiency as a function of helio-centric distance; and

(vi) detection of OD and the determination of an upper limit on N(OD)/N(OH).

3.2. COOL STARS

3.2.1. *T Tauri stars*

The observations of UV spectra of T Tauri stars and Herbig type Be- and Ae-stars in dark nebulae have provided new insight to the physics of pre-main sequence stars. The UV spectra have revealed high temperature chromospheres around some pre-main sequence stars, the highest ionization stage observed in emission is N v (λ1240)

formed at 2×10^5 K. All T Tauri stars have C IV (λ1550) in emission besides lines of O I, C I, C II, C III, Si II, Si III and Si IV and a suspected He II line in the spectrum of T Tau (Gondhalekar *et al.* 1979). Hence the line emitting regions around T Tauri stars cover a large range in temperature—from 7×10^3 K to 2×10^5 K. The UV spectrum between 1900 Å and 3000 Å is dominated by emission line in some cases and by absorption lines in others, although Mg II (λ2800) line is always seen in emission. The wavelength for the onset of chromospheric emission line spectrum is different for different stars; in the spectrum of V380 Ori, a star of earliest spectral type observed, the absorption line spectrum extends down to 1250 Å but in RW Ori emission lines have been detected shortwards of 3000 Å (Imhoff & Giampapa 1980; Cram 1980). A continuum emission is seen in all spectra, but the short wavelength limit of the continuum emission is different for each star. In all stars, except the two earliest types (V380 Ori and HR 5999), the continuum emission has strong excess over photospheric emission and can be explained as Balmer continuous emission in the emitting volume around a star.

Simultaneous infrared, visible and UV spectra of T Tauri stars are required to study the variability of pre-main-sequence stars and establish correlations between emission in different wavelength bands. However, it is perhaps significant that inspite of the large range in observed parameters like C IV luminosity or widths of emission lines, the densities in the line emitting regions do not differ by more than a factor of two from the average value.

3.2.2. *Chromospheres and coronae*

Before the launching of satellite observatories, chromospheres and coronae of several late type stars were modelled principally from observations of Ca II H, K lines and to a lesser degree continuously (de Jager *et al.* 1978) and simultaneous visible data obtained from various ground based observatories. This was a program of investigation of very short time scale variations in the winds of early type supergiants, with a view to understanding mass loss mechanism, the high degree of ionization and the stellar wind. A remarkable change in the wind velocity of 100 km s^{-1} in half an hour can be seen from the blue wind of N V (λ1240) line observed in the spectrum of α Cam. These observations suggest that there are gradual short term changes in the terminal velocity of the wind and these changes increase with increasing distance from the star. The changes in the wind speed may be due to changes in the UV flux from a star or changes in the mass loss rate. These changes also establish that there are short term very rapid changes in the wind speeds with the largest change being observed in the lines of ions of high ionization potential.

The mass loss and stellar winds in homogeneous groups of early O stars have been studied from the UV spectra of these stars in clusters (Burki *et al.* 1978). The P Cygni profiles of N V (λ1240), C IV (λ1550) and N IV (λ1718) lines indicate that the mass loss rates range from 10^{-6} $M_\odot$ yr^{-1} to 2×10^{-9} $M_\odot$ yr^{-1}. But the correlation between the mass loss rate and bolometric lumonosity has not been firmly established; Burki *et al.* (1978) find a linear relation between mass loss rate and M_{bol} as predicted by line-radiation-driven wind theory but Conti *et al.* (1980) show from their study of a large sample of stars that the mass loss rate can differ by a factor of 50 for a given M_{bol}. Clearly, further observations and theoretical development are required to explain the mass loss rate satisfactorily.

3.2.3. Mass loss from hot subdwarfs

Mass loss from O- and B-type stars brighter then $M_{bol} \simeq -6$ has been known for some-time (Snow & Morton 1976), but the mass outflow from hot subdwarfs, comparable in temperature to the hottest O stars but considerably less luminous was an unexpected discovery (Darius et al. 1979). Figure 5 shows the low resolution spectra of three subdwarfs with mass from balloon observations of Mg II H, K lines. Although these diagnostic techniques have been carefully developed and extensively used, these two spectral lines are sensitive probes for only the lower regions of stellar chromospheres where $T < 7000$ K. In UV spectra, the lines of Si II, Si III and C II, which are formed in the 5000–20000 K temperature region, can be observed.

UV spectra of many late type stars have been obtained (Brown et al. 1980; Linsky et al. 1979; Ayres & Linsky 1980; Simon et al. 1980; Hartmann et al. 1980) and previously undetected weak emission features observed. The spectra of these stars clearly indicate two distinct groups of stars : (i) a solar type group in which high temperature lines are observed, indicating a chromosphere, a transition region and a high temperature corona, and (ii) a non-solar type group in which only low temperature lines are observed, suggesting a chromosphere only. The distinction between stars with "hot" and "cool", chromospheres can be seen in the HR diagram of Figure 6 (Paschoff et al. 1979). The change in the character of the outer atmospheres of the two types of stars can be interpreted as being due to either the absence of hot material resulting
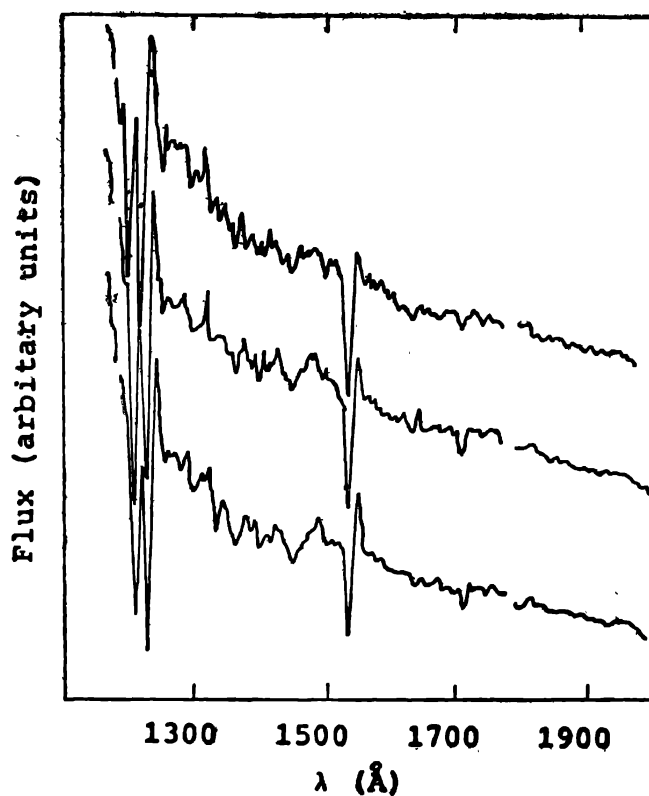

Figure 5. IUE spectra (low resolution) of three hot subdwarfs showing mass loss (Darius et al. 1979).

from the onset of stellar wind (possibly L_α driven) (Mullan 1976; Linsky *et al.* 1979) or to very low transition region densities. But the distinction between the hot transition region stars and the cool chromosphere stars may not be as sharp as that indicated in the HR diagram of Figure 6 (Harthmann *et al.* 1980). The strong blue shifted absorption in Mg II lines and the detection of high temperature lines in α Agr(G2Ib) and β Agr (G0Ib) indicate that the presence of high mass loss does not rule out high temperature and that the transition from "solar type winds" to "supergiant winds" must be more gradual.

3.3. HOT STARS

3.3.1. *Mass loss from early type O stars*

The mass loss from early type hot stars has also been a topic of intense study with data obtained with IUE. The UV spectra of α Cam O9.5 Ia and κ Cas B1 Ia were monitored for 72 hours loss characteristics. The P Cygni profiles of C IV line λ1550 are clearly seen in this Figure; the relevant stellar parameters of these stars are given in Table 4. Although the hot subdwarfs fail to meet the luminosity criteria established
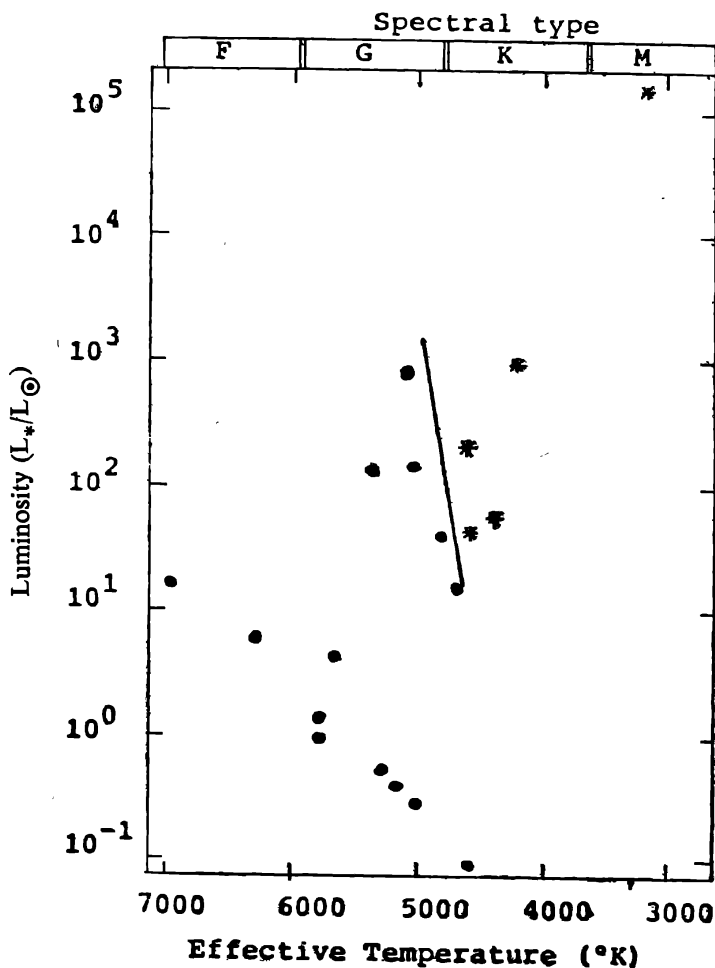

Figure 6. HR diagram for cool stars; (●) hot corona stars, (*) cool chromosphere stars (Paschoff *et al.* 1979).

Table 4. Stellar parameters of mass losing binaries

	BD +37°1977	BD +37°442	BD −3°2179
V	10.2	9.99	10.37
T_{eff} (°K)	55000	55000	55000
log g (cm s^{-1})	4.0	4.0	4.5
log $(L/L_{\odot})$	4.4	4.4	3.9
Γ	0.66	0.66	0.19
V_e (km s^{-1})	280	280	580

Γ = stellar luminosity/Eddington limit.
V_e = escape velocity.

for mass loss from massive OB stars, these stars do appear to satisfy the luminosity-to-mass criterion established for central stars of planetary nebulae.

3.4. INTERSTELLAR MEDIUM (GALACTIC)

3.4.1. *Interstellar gas*

Observations from space based observatories have significantly affected studies of the interstellar medium. A few years ago the interstellar medium was believed to consist of cool ($T < 100$ K) "clouds" embedded in diffuse "warm" ($T \sim 10^4$ K) intercloud medium of partially ionized hydrogen. An adequate source of ionization and heating was however not known and low energy cosmic rays, soft x-rays and hard UV radiation were considered possible and equally likely sources. *Copernicus* observations of interstellar O VI and observations of soft x-ray background radiation indicate a "hot" phase of interstellar medium. The observations of interstellar medium with *Copernicus* (Spitzer & Jenkins 1975) and the hot shocked plasma of "violent interstellar medium" (McCray & Snow 1979) have been reviewed elsewhere.

While the observations of interstellar UV lines by *Copernicus* were limited to relatively bright stars within about 3 kpc of the Sun with IUE it is possible to obtain high resolution ($\Delta\lambda/\lambda \sim 1.2 \times 10^4$) UV spectra of moderately reddened stars as faint as $m_v \simeq +13$. It is thus possible to probe the hot gas both in the galactic disc and the galactic halo to greater distances than was possible before, and although the O VI line $\lambda 1034$ is not accessable to IUE, it is possible to observe resonance lines of Si III($\lambda 1206.5$), Si IV ($\lambda\lambda 1393.8, 1402.8$), C IV ($\lambda\lambda 1548.2, 1550.8$) and N V ($\lambda\lambda 1238.8, 1242.8$) and probe the intermediate temperature range $3 \times 10^4 < T < 3 \times 10^5$ K. Surveys of limited sample of stars (Black *et al.* 1980; Bromage *et al.* 1980) indicate that the strengths of these lines are inconsistent with their formation in the same hot gas responsible for O IV line. There is no "grand design" immediately obvious in the spatial distribution of C IV column densities, and there is no close correlation between C IV and Si IV column densities with distance. This lack of correlation is similar to the lack of correlation found for O IV, and implies that a major contribution to C IV and Si IV column densities is from relatively small number of localized sites such as cloud conductive interfaces (Cowie *et al.* 1979). Model calculations of Black *et al.* (1980) have shown that the column densities of Si IV and C IV observed in their sample of 25 stars can be explained by normal photoionized H II regions and the lines of these ions may be formed in the H II regions of stars observed as background sources. However, the N V lines observed in the spectra of these stars must

arise in the same gas responsible for the O VI line and this highly ionized material must be truly interstellar. Two competing interpretations of the highly ionized material are available, global and circumstellar. In both interpretations, O VI is formed by collisional ionization; in the global model the hot material is maintained by mechanical energy injected by supernova shock waves and in the circumstellar model, by interaction with stellar wind. Elaborate statistical tests are needed to distinguish between these two models, and the sensitivity and the wavelength coverage of IUE permit observations of previously inaccessible regions of the disk and the halo of the Galaxy to make such tests possible.

3.4.2. *Galactic halo*

The existence of a galactic halo of hot gas has been discussed by many authors (Spitzer 1956; Sciama 1962; Weisheit & Collins 1976; Chevalier & Oegerle 1979). The narrow absorption lines at arbitary redshifts found in the visible spectra of high redshift quasars and BL Lac objects (Boksenberg 1978) are believed to be formed in the halos of intervening galaxies. However, a definite association of high excitation lines like C IV and Si IV with galactic halos was not established. High signal to noise ratio spectrum of quasar 3C273 ($b^{II} = 64.4$) has narrow absorption lines at zero redshift (Ulrich *et al.* 1980); these lines must be formed in the halo of our Galaxy. The observation of strong C IV absorption line in this spectrum resolved the aparent anomaly that interstellar C IV in our Galaxy observed with hot stars as background sources is weak but C IV observed in the spectra of high redshift quasars is strong. Clearly, the total column of C IV in the halo of our Galaxy is of the same order as that in the halos of other galaxies. This hot gas is at high z above the plane of the Galaxy in a region of halo which cannot be probed with hot stars as background sources.

The galactic halo in the direction of Magellanic Clouds and indeed the halo around the Clouds and the gas in the intergalactic space has been probed by observing spectra of early type hot stars in Magellanic Clouds (Savage & de Boer 1979; de Boer & Savage 1980; Gondhalekar *et al.* 1980; Savage & de Boer 1980). The lines of sight to these extragalactic stellar sources do not pass close to or through H II regions of galactic stellar sources and the absorption lines at 0 km s⁻¹ (the absorption lines due to gas in the LMC would be formed at +270 km s⁻¹) are obviously formed in the halo of our Galaxy with some contribution from the galactic disc. The detection of C IV and Si IV lines in the spectrum of quasar 3C273 (a source in the northern hemisphere) and in the spectra of Megallanic Cloud stars (sources in the southern hemisphere) confirms the global distribution of hot gas in the halo of our Galaxy.

3.5. HIGH ENERGY OBJECTS

3.5.1. *X-ray binaries*

The only x-ray binary observed in UV before the launch of IUE was X Per, as all other x-ray binaries were too faint to be detected at UV wavelengths with pre-IUE satellite observatories. International collaboration has enabled more valuable data to be collected on x-ray binaries in last two years than would have been

P. M. Gondhalekar

Table 5.

x-ray obj.	Optical obj.	Sp. type	m_v	log L_x	L_x/L_{op}	Period
Massive x-ray binaries						
1700 − 37	HD 153919	O.6.5f	6.6	36.5	0.0005	3.41^d
Veal X-1	HD 77581	B0.5Ib	6.9	36.0	0.003	8.97
Cyg X-1	HDE 226868	O.9.7Iab	8.9	37.3	0.02	5.60
SMC X-1	Sk 160	B0 I	13.3	38.3	1.2	3.89
LMC X-4	Ph-Sk	O8III-V	14.0	38.7	1	1.41
0352 + 30	X Per	O9.5(III-V)$_e$	6.0	34.0	0.0001	581?
1145 − 61	Hen 715	B 1V ne	9.0	36.8	0.2	?
Low mass x-ray binaries						
Sco X-1	V818 Sco	blue	12-13	37.3	600	0.79
Cyg X-2	V1341Cyg	A–F	15.5	37.7	450	9.84
Her X-1	HZ Her	A–F	13-14	37.0	10	1.7
1814 + 498	AM Her		12-13	33.9	0.6	0.13

possible if individual groups had obtained data separately. Simultaneous ground based and x-ray observations were also possible. The x-ray binaries observed with IUE are given in Table 5 (Hammerschlag-Hensberg 1980).

The emission of x-rays in a binary system, where matter from a primary accretes on a compact secondary, has been known for some time. Optical studies of x-ray binaries had shown that ultraviolet observations would clarify uncertainties about mass loss rates from the primary, the stellar wind properties, and the luminosity of the accretion disk round the secondary. If the primary of a binary system is a supergiant, then the x-ray emission from the stellar wind accreting on the secondary would modify the ionization structure of the stellar wind (McCray 1975). The ionization of stellar wind by x-rays would be observable as a marked phase dependence of P Cygni profiles of resonance lines of Si IV, C IV and N V; such phase dependence can be clearly seen in the Si IV lines of HD 77581 (Vela X-1) (Dupree *et al.* 1980). The spectrum obtained at high resolution shows that at x-ray eclipse (zero phase) the Si IV line has an extended blue wing with an edge velocity ∼1700 km s^{-1} and little or no evidence of emission. At phases of 0.44 and 0.52, the edge velocity has dropped to ∼850 km s^{-1} with increased emission. Similar high resolution observations of Si IV and C IV resonance doublets in the spectra of 1700−37/HD 153919 show no phase dependence of line profiles; this may indicate high optical depths in the C IV and the Si IV lines and the lines would be completely saturated making detection of x-ray ionization difficult. Unfortunately, not all massive binaries can be observed at high resolution, but comparision of low dispersion spectra of Vela X-1, Cyg X-1, SMC X-1 and LMC X-4 show that the phase dependence of the equivalent widths of the resonance lines in the spectra of these stars is in qualitative agreement with x-ray modification of stellar wind.

The accretion disk component in UV emission has been observed in the spectra of low mass binary system Her X-1/HZ Her (Gursky *et al.* 1980). This close binary system consists of a late A type star (∼2 $M_\odot$) and a neutron star (∼1 $M_\odot$). The binary period is 1.7 days during which the optical spectrum varies between A7 and B0 (x-ray heating of the primary). A 35 day period has also been found (x-rays ON for 11 days and OFF for 24 days) and is attributed to the precessing accretion disk

round the neutron star. The UV continuum flux shows precisely these two periods— a 1.7 day variation due to heated photosphere of the primary and a 35 day variation due to accretion disk with the disk visible during the eclipse of the primary.

3.5.2. *Supernova*

The type II supernova (SN) 1979c ($m_B \doteq 12$) in the Sbc 1 spiral galaxy M100 (NGC 4321) provided an ideal opportunity to follow the evolution of UV spectrum of a supernova explosion. Simultaneous optical, radio and x-ray observations were also made to provide a complete coverage of the explosion over a large energy range. These data are still being reduced and analysed and only a brief account of the UV data is given here.

The SN 1979c is located close to the main spiral arm of M100 and almost coincident with an H II region seen on a pre-explosion plate. The association with a spiral arm and proximity to an H II region suggests that this is a typeII SN and this classification is confirmed by the evolution of the optical spectrum (Branch *et al.* 1980). This SN was brighter than any previously observed type II SN and a series of UV spectra at low resolution ($\Delta\lambda \sim 6$ Å) were obtained from 1979 April 22 to 1979 August 4. A colour excess of $\sim$0.1 $\pm$ 0.03 was estimated from the well known 2200 Å extinction feature and a colour temperature of 11000 K was estimated from the continuum energy distribution. A large fraction of UV radiation is emitted as continuum flux rather than line flux. A comparison of x-ray, UV, optical and infrared emissions indicated that 44.4 per cent of radiation was emitted in the 1160–3200 Å band, and only 1.5 per cent at wavelengths shorter than 1160 Å. The light curve declined at the rate of 0.046 mag day^{-1} in the B band and at the rate of 0.181 mag day^{-1} in a band 100 Å wide centered at 1300 Å, indicating a colour temperature drop from 11000 K on 1979 April 22 to $\sim$7400 K on 1979 May 7. After mid-May the rate of decline in the UV decreased, becoming similar to that in the B band and indicating a constant photospheric temperature after mid-May.

The absorption lines observed in these spectra are interstellar lines, which are formed in M100 and in our own Galaxy. Both low ionization (e.g. O I, C I, C II, Mg II) lines and high ionization lines (e.g. Si IV, C IV) are observed. The velocity dispersion of the neutral and singly ionized lines is in the range of 16–25 km s^{-1} but the velocity dispersion of highly ionized lines is of the order of 50 km s^{-1}. The prominent emission lines observed in the spectra of SN are the resonance lines of N v, Si IV, N V and the inter-combination lines of N III (1750 Å) and C III (1909 Å). The detection of N IV (1715 Å) line, a permitted transition between excited levels, indicates an overabundance of nitrogen; it is found that N/C $\sim$7 and O/C $<$4 (Panagia *et al.* 1980). The enrichment of N or the depletion of C and O implies nuclear processing through a non-equilibrium CNO cycle which can occur in the H-burning shell during the red giant phase of the progenitor star. The profiles of high ionization lines like C IV are distinctly different from the profiles of low ionization lines like Mg II and H$_\alpha$. The symmetric C IV line has a velocity displacement of about 1800 km s^{-1} but the asymmetric H$_1$ profile has a flat topped blue wing extending to $-$5000 km s^{-1} and the red wing drops steadily from 0 km s^{-1} to $+$9300 km s^{-1}. The expansion velocity is close to the velocity obtained from optical lines and the receding part of the H$_\alpha$ emitting region is obscured by the SN

photosphere. The shell emitting high excitation lines is physically separated from the SN photosphere and has distinctly different velocity and excitation conditions. The UV line emitting material is probably ejected from the stellar progenitor as stellar wind, which is subsequently compressed, heated and accelerated by the SN explosion.

3.6. NORMAL GALAXIES

3.6.1. *Galactic dust*

The wavelength dependence of interstellar extinction in the visible and the UV regions is determined by the composition and the abundance of the agents responsible for scattering and absorption. The UV extinction in our Galaxy has been studied in great detail over last few years from stellar data obtained with satellite observatories (Nandy *et al.* 1976 and others). However, the determination of UV extinction law of the Large Magellanic Cloud from surface brightness measurements with the S2/68 (Nandy *et al.* 1979) experiment on TD1 satellite and the measurements with the ANS satellite (Borgman 1978) led to ambiguous results. This ambiguity has been resolved from IUE observations of reddened and unreddened stars in the Clouds (Nandy *et al.* 1980). These astronomers have determined the extinction in the Large Magellanic Cloud particularly around 30Doradus region and in the bar. The striking difference in extinction in LMC compared to the mean extinction in the Galaxy can be seen in Figure 7, the wellknown 2200 Å absorption feature is very weak or absent around 30Doradus and the extinction in the bar is significantly different from the extinction around 30Doradus but is similar to the mean galactic extinction. The increased UV extinction around 30Doradus probably indicates that the relative abundance of small (a few hundred angstroms) dielectric particles is significantly greater than the relative abundance of such particles in the interstellar medium in the solar neighbourhood.

The UV extinction properties of dust in Magellanic Clouds can be determined from observations of individual stars in the Clouds but this is not possible at present for more distinct extragalactic systems. For such systems, the extinction properties of dust in and around the source of UV radiation can only be determined from the observed line intensities and the presence or otherwise of the 2200 Å absorption feature in the continuum. Both methods assume that the extinction law in the extragalactic systems would be similar to the extinction law in our Galaxy and determinations of colour excesses have been predictably ambiguous. The line intensity method fails because the most dominant lines in the visible and the UV spectra of extragalactic systems, namely the hydrogen lines, are not radiative, and because the high density and the high opacity modify the line intensities far more severely than any reddening effects. The 2200 Å feature is usually weak in the spectra of extragalactic objects, or it can be mimicked either by Fe II emission between 2300 Å and 2800 Å or by the stellar composition of a Galaxy (Bertola *et al.* 1980). An exception appears to be the extragallactic H II region Tololo 1924-416 ($z = 0.0096$). In the UV spectrum of this object (Gondhalekar *et al.* 1980), the 2200 Å feature is clearly present, and the colour excess obtained by dereddening the spectrum with a mean galactic extinction law (Seaton 1979) is 0.43 $\pm$ 0.05. The colour excess
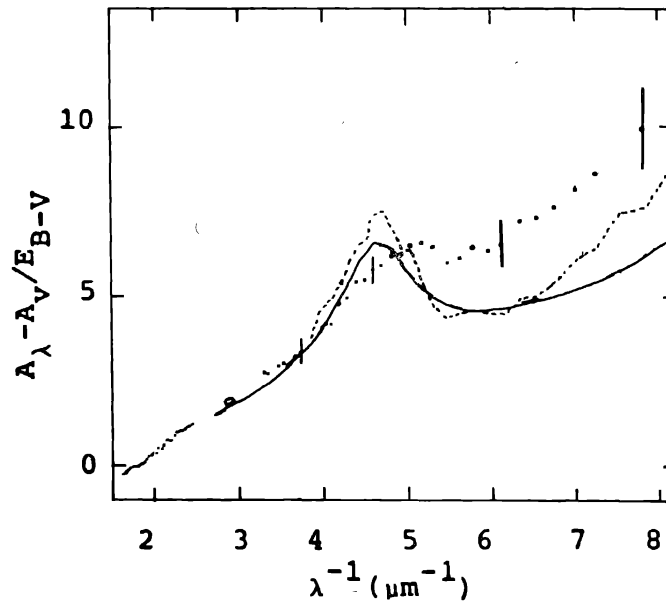
Figure 7. Extinction curves for Large Magellanic Cloud; (○) U band data, (·) mean extinction curve for 30Doradus, dashed line denotes extinction curve in the bar and the solid line is the mean galactic extinction curve (Nandy *et al.* 1980).

determined from the intensity of Balmer lines is 0.52 ± 0.10; considering the errors and the uncertainities involved in these two determinations, this agreement is remarkably good. The galactic reddening in the direction of Tololo 1924-416 is low $(E_{B-V} < 0.05)$ and no interstellar absorption lines are observed in the UV spectrum (for a colour excess of 0.43, the galactic interstellar absorption lines should be very strong); it seems reasonably certain that the 2200 Å absorption feature is produced by dust around the source of continuum radiation, and the extinction properties of this dust are very similar to the extinction properties of the dust in our Galaxy. The dust surrounding the line emitting region (which may be removed from the source of continuum radiation) is also similar to the galactic dust.

3.6.2. *Interstellar medium and galactic halo*

The interstellar gas, in our nearest extragalactic neighbours, the Magellanic Clouds, has been detected in spectra of early type hot stars in the Clouds (de Boer *et al.* 1979; de Boer & Savage 1980; Gondhalekar *et al.* 1980). In these spectra, strong absorption lines are observed at the radial velocities of Clouds. The velocity structure of the Cloud ISM and the Cloud halo is not simple nor is it well understood. Also quantitative information on the ISM is difficult to obtain. But the extended blue wing of the lines of highly ionized ions shows that the hot ($\sim 10^5$ K) gas tends to be in the outer regions of the halo, and this is in qualitative agreement with the location of hot gas in the halo of our Galaxy.

The halos of distant extragalactic systems can be probed by observing the spectra of background objects. The line of sight of the QSO 3C232 ($z = 0.53$) passes within 90 arcsec of the nucleus of the spiral galaxy NGC 3067. Ca II and 21 cm absorption

due to this galaxy have been detected in the spectra of 3C232 (Boksenberg *et al.* 1978; Haschik and Burke 1975). Strong Mg II and weak Fe II and Si II absorption lines due to NGC 3067 have been detected in the UV spectrum of 3C232 but the lines of C IV and Si IV are almost certainly absent (Snijders 1980). The line of sight to Mkn 205 ($z = 0.071$) passes within 40 arc sec of the nucleus of the spiral galaxy NGC 4391 ($z = 0.007$). In the UV spectrum of Mkn 205, the absorption lines of neutral or singly ionized atoms (O I, C II, Mg II and Al II) have been detected (Gondhalekar & Wilson 1980a), but again the resonance lines of C IV and Si IV are either weak or absent.

3.6.3. *Ultraviolet continuum of elliptical and spiral galaxies*

An accurate evaluation of the stellar content of elliptical and spiral galaxies is becoming increasingly important as the history of star formation, particularly in elliptical galaxies, can now be modelled theoretically. The correction for stellar populations is the least certain factor in the determination of the cosmological deceleration parameter from observations of distant galaxies. The synthesis of stellar populations of galaxies from optical photometric data is a well established technique (*e.g.* O'Connell 1976) although the results are not always unique (Peck 1980). The optical continuum flux from elliptical galaxies or the nuclei of spiral galaxies can be matched with the continuum flux emitted by cool stars (Bertola *et al.* 1980; Ellis & Gondhalekar 1980). But very little or no information about the population of hot O- or B-type stars or hot horizontal branch stars in the galaxies is available from the optical data. The presence of hot stars in galaxies is illustrated by the sharp increase in UV continuum radiation below 2000 Å (Code & Welch 1979; Bertola *et al.* 1980) shown in Figure 8. The continuum between 2000 Å and 1200 Å can be fitted by a black body at 30000 K and the large spatial extent of this increase in the continuum flux suggests an extended distribution of stellar sources rather than a massive point source (Young *et al.* 1978; Sargent *et al.* 1978). It is interesting to compare the spectrum of M87 with those of M31 and M32 (Johnson 1979), the wavelength of the minimum in the UV spectra is different in the three galaxies, indicating a relative change in the proportion of hot stars. Similar minima, followed by rapid increases, are observed in the UV spectra of the nucleii of spiral galaxies (Ellis & Gondhalekar 1980), but no such minima are observed in the spectra of massive H II regions in spiral and irregular galaxies (Gondhalekar *et al.* 1980), indicating a more homogeneous stellar populations in H II regions.

The computations of K-corrections for galaxies have been limited by lack of information concerning the energy distribution of galaxies in the UV region. Recently, Pence (1976) has presented K-corrections for a number of morphological types based largely on the preliminary OAO stellar data. These corrections have been recalculated with data on photometry of two galaxies (Code & Welch 1979) with widely different energy distributions. The results show that the K-corrections for the two energy distributions diverge with increasing z and as $z \to 1$ the divergence becomes equal to the typical evolutionary change in the visual magnitude. The K-correction calculations did not include evolutionary effects, nor is it possible to separate evolutionary effects in K-corrections as the UV flux is an input parameter for calculations of galactic evolution. It may be that the galaxies which have significantly different UV luminosities evolve from states which had a similar UV
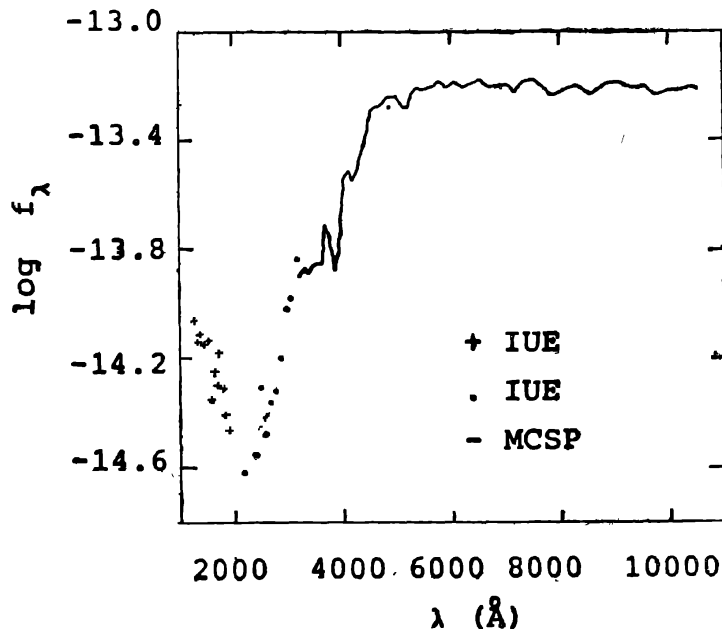
Figure 8. Visual and ultraviolet energy distribution of the nucleus of M87 (Bartola *et al.* 1980).

luminosity and if this is so, then the scatter obtained by Code & Welch (1979) would disappear at higher redshifts and K-corrections would still be meaningful. If, however, the excess UV flux is due to hot stars, than the evolution time would be short on the Hubble time scale, and the UV data would impose an irreducible uncertainty on any K-correction at large redshift.

3.7. ACTIVE GALAXIES

The UV observations of active galaxies are valuable in revealing the presence of hot star population, an ionizing non-thermal source and resonance emission lines which provide information on the physical state of the ionized gas. UV observarions of active galaxies were started with ANS observations of QSO 3C273 and the type 1 Seyfert galaxy NGC 4151. The interpretation of QSO data was hampered by the low resolution, but the data on NGC 4151 are valuable for study of long term variability of this object. A systematic study of the UV spectra of active galaxies was initiated after the launch of IUE, and a wealth of data on quasars, Seyfert galaxies and BL Lac objects has accumulated in the last two years.

3.7.1. *Seyfert galaxies and quasars*

The anomalous L_α/H_β emission line ratio of hydrogen in low redshift quasars and Seyfert Type I galaxies has been studied extensively (Baldwin *et al.* 1978; Boggess & Wu 1979; Ferland *et al.* 1979; Oke & Zimmermann 1979; Ulrich *et al.* 1980), and the combined average result is that the ratio is around six with very small dispersion. This is lower by a factor six than the simple approximation of Case B recombination theory. This ratio is similar to the ratio found for high redshift quasars (Baldwin 1977). The H_α/H_β ratio and P_α/H_β ratio on the other hand are nearly consistent

P. M. Gondhalekar

with the prediction of recombination theory (Puetter *et al.* 1978). The L_α/H_β ratio for the narrow line region seems more nearly normal. A general difficulty in interpreting these results is the role of dust in destroying the resonantly trapped L_α photons; however, several lines of evidence argue against dust as the sole agent responsible for destroying L_α photons. The 2200 Å absorption feature is seldom detected in spectra of quasars or Seyfert galaxies at strength comparable to that observed in the spectrum of 3C120, Mkn 79 or Tololo 1924-416, and may be mimicked by weak Fe II emission at longer wavelengths. Dust reddening can also be determined from the He II ($\lambda 1640$)/$\lambda 4686$) line ratio and O I ($\lambda 1302$)/($\lambda 8446$) line ratio, but in a large number of objects, the H II line ratio deviated (Gondhalekar *et al.* 1980) in the sense that He II ($\lambda 1640$) line is *stronger* than the value predicted by the recombination theory and effectively arguing against reddening. In the spectrum of 3C273, the O I line ratio yields $E_{B-V} = 0.26$ (Davidsen 1979), a value considerably higher than that determined from the 2200 Å feature (Ulrich *et al.* 1980). It is, of course, possible that the reddening law in active galaxies is significant different from the galactic reddening law.

A different approach to the problem is to consider the energy budget—selective distruction of L_α radiation would lead to a significant excess of ionizing photons over the number of L_α photons produced by recombination. For 3C273, if all Lyman continuum photons are converted to Balmer line emission plus L_α, then H_β would be deficient by a factor of 2–4 and L_α by 10–20. If H_β flux is used as a measure of covering factor, then L_α is suppressed by a factor of 5, but if a statistical covering factor of 10 per cent is used, then L_α is approximately consistent with the recombination theory, but H_β is enhanced by up to a factor of 5. The enhancement of H_β is favoured in the analysis of the broad line radio galaxy 3C390.3 (Ferland *et al.* 1979).

Observations of quasar spectra at wavelengths shorter than the Lyman limit have the potential of detecting XUV resonance lines of He I ($\lambda 548$), H II ($\lambda 304$), C III ($\lambda 977$), Mg X ($\lambda 609$), Ne VIII ($\lambda 770$) etc. A positive detection of He II resonance line would lead to a better understanding of the hydrogen line emission since the two atomic systems are isoelectronic. The detection of C III resonance line along with semiforbidden C III] line $\lambda 1909$ (which is observed in the spectra of all quasars) allows immediate conclusions to be drawn about the electron density N_e and the electron temperature T_e. However, the C III] resonance line has been detected only in the spectrum of Q1011+25 (Ton 490 $z = 1.63$) (Gondhalekar & Wilson 1979). The C III] ($\lambda 977$)/($\lambda 1909$) line ratio has been interpreted by Nussbaumer and Schild (1979); the electron densities and the corresponding temperature determined by these authors are

T_e (°K)	N_e(cm^{-1})
30000	$< 10^9$
15000	$> 3 \times 10^{10}$
10000	$\simeq 10^{12}$

These densities are considerably higher than the values usually assumed for the C III] line emitting region in quasars.

High redshift quasars provide a probe for the intergalactic medium and the intervening gas associated with galaxies and clusters. The continuum flux below He I ionization edge at λ504 Å has been detected in the spectra of three quasars (Boggess *et al.* 1979; Green *et al.* 1980). The near transparency of the intergalactic medium at these wavelengths indicated by these observations requires the gas in the intergalactic medium to be ionized.

3.7.2. *BL Lac objects*

The absence of emission lines in the spectra of BL Lac objects has been a puzzle for a long time. Observations of UV spectra have established that ionizing photons are present in these objects (Kondo *et al.* 1980; Snijders *et al.* 1980; Bromage *et al.* 1980). Even the dominant UV resonance lines are not observed in the spectra of these objects, and it must be concluded that this absence of emission lines is due to the absence of emitting gas. The combination of power-law spectrum, linear polarization of optical light, and rapid time variation suggests a synchrotron origin of some of the continuum radiation in BL Lac objects.

The near simultaneous observations at radio, infrared, optical, UV and x-ray frequencies of Mkn 501 (Snijders *et al.* 1980) indicate a power law spectrum from UV to x-ray, and the spectrum steepens towards very hard x-rays. A crucial step in the analysis of these data is the separation of the power law from the dominant contribution in the optical and the infrared by the galaxy surrounding the active nucleus. By removing a standard galaxy energy distribution, the power law appears to flatten in the near UV and the visible. This spectral flattening can be interpreted as reflecting radio spectral turn over and the optical, UV and x-ray photons produced by "self-Compton" scattering of radio photons off relativistic electrons. The steepening towards hard x-rays would suggest high energy cut-off in relativistic electrons at ∼4 GeV. These data do not rule out other models, *e.g.,* inverse Compton scattering off thermal electrons.

3.7.3. *Gravitational lens*

The twin quasars 0957+561 A, B were discovered close to their radio positions by Walsh *et al.* (1979). The quasars have identical emission line redshifts ($z = 1.41$) and absorption line redshifts ($z = 1.39$). The spectra of the two quasars are also similar in the strengths of the emission lines, absorption lines and continua. The remarkable similarity of the two spectra led Walsh *et al.* (1979) to propose that they were two images of one quasar and that the images were formed by an intervening massive galaxy acting as a gravitational lens. Since this discovery paper, extensive observations of the twin quasars have been made, both in the optical and the radio regions (Weymann *et al.* 1979; Wills & Wills 1980; Pooley *et al.* 1979; Roberts *et al.* 1979; Porcas *et al.* 1979; Greenfield *et al.* 1980), and these observations are consistent with the gravitational lens hypothesis. The discovery of an elliptical galaxy of red magnitude 18.5 superposed on the southern component of the twin quasar has been reported by Gunn *et al.* (1979). This galaxy is the brightest member of a rich cluster of galaxies. The lensing geometry due to the gravitational field of the elliptical galaxy and the cluster has been discussed by Young *et al.* (1979). A contribution from the intervening elliptical galaxy to the flux from the twin system
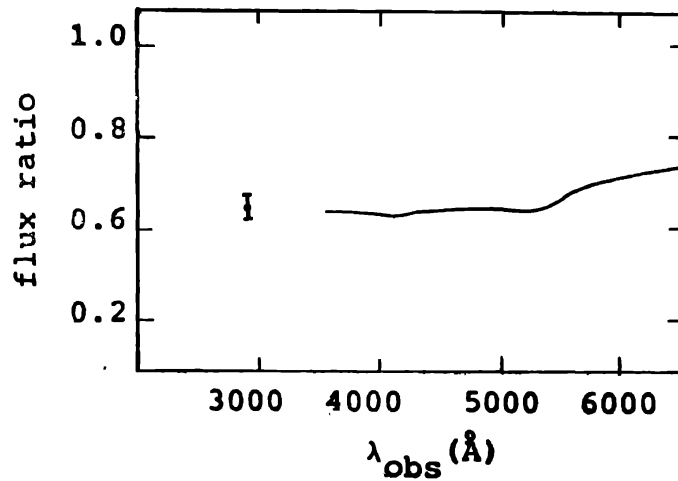
P. M. Gondhalekar

Figure 9. The ratio of fluxes for 0957+561 (south) to flux from 0957+561 (north) (Gondhalekar & Wilson 1980).

has been detected by multichannel spectrophotometric observations (Young *et al.* 1979). From the location of the characteristics Ca II (λ 3950) break (observed in the spectra of elliptical galaxies), a redshift of 0.39 was derived for the lensing mass. On the bases of this prediction, the second less conspicuous feature at 4000 Å (Figure 9) can be identified as the Mg II (λ 2800) break, also observed in the spectra of elliptical galaxies.

If the lens hyphothesis is correct the ratio of fluxes from the two images should be constant at all wavelengths but the intervening elliptical galaxy would make substantial contribution in the visible and the infrared (Lebofsky *et al.* 1980). The structure in the ratio of the visible fluxes led Walsh *et al.* (1979) to suggest differential extinction of the two light paths causing a reddening of the southern component relative to the northern component. UV spectra of the twin quasars (Gondhalekar & Wilson 1980b) coupled with radio observations confirm the constancy of the ratio of fluxes in the region of the electromagnetic spectrum where elliptical galaxies make negligible contribution. The ratio of the flux ratios in the two frequency ranges is 0.94 $\pm$ 0.06. For a galactic extinction law, this ratio leads to an upper limit of 0.04 for colour excess between the two light paths. This low value almost certainly means that the two light paths are extinction free either because the intervening galaxy is dust free or the light paths pass through the dust free halo of the galaxy. The value of unity for the ratio of the ratio of fluxes in the UV and the radio regions provides strong evidence in favour of the gravitational lens hypothesis.

4. Conclusions

UV astronomy has been revolutionised since the launch of IUE, and only a small fraction of data has been reviewed here. What has been established beyond doubt is that the observatory mode of satellite operations is both feasible and the most efficient way of using space based observatories. The real-time participation of an astronomer makes extensive pre-preparation unnecessary and also prevents

accumulation of irrelevant data. With the success of IUE in mind, a follow-on mission for ultraviolet astronomy in the next decade has been proposed, both at the European Space Agency in Europe and at the National Aeronautic and Space Administration in the U.S.A. The basic concept is to launch a metre class telescope with a Image Photon Counting detector in a IUE like configuration, but with an additional requirement that the detector also be sensitive to radiation between 912 Å and 1200 Å. The proposals were discussed at two well attended meetings organised to coincide with the 'Second European IUE Conference' at Tubingen, Germany, and the 'Symposium on the Universe at Ultraviolet Wavelengths : The

Table 6

Payload	Launcher	Scientific objective	Telescope	Mode
Febry-Perot interferometer	Balloon	High resolution spectroscopy around 2800 Å	40 cm	Spectroscopic ($\Delta\lambda/\lambda = 1.5 \times 10^5$)
Echelle spectrograph	Balloon	High resolution spectroscopy in the 1950–3300 Å region	31 cm	Spectroscopic ($\Delta\lambda/\lambda = 4 \times 10^4$)
Wide field telescope	Rocket	Ultraviolet images of extended sources	33 cm	Filter photometry
Wide field telescope	Space lab	Ultraviolet images of extended sources	38 cm	Filter photometry
UFT	Satellite	Galactic and extragalactic spectroscopy	80 cm	Spectroscopic (resolution 0.2-0.4 Å)
FAUST	Satellite	Low resolution spectroscopy Wide field photometry		Spectroscopie (8 Å) Photometric (250 Å)
FOS	Satellite	Wide field images		UV images at 1550 Å
Schmidt-Cassegrian telescope	Balloon	Wide field images		UV images in the 1850–2100 Å region

Status	Agency
Operational	Queen's University, Belfast, N. Ireland, U.K. (Bates *et al.* 1979)
Proposed 1980	University College London, London, U.K.
Operational	NASA-Goddard Space Flight Center (Stecher and Bohlin 1980; Hill and Bohlin 1980)
Proposed	NASA-Goddard Space Flight Center
Proposed 1982	Laboratoire de Physique Stellaire et Planetaire, France France-USSR collaboration
Proposed	Laboratoire de Physique Stellaire et Planetaire, France
Proposed	Laboratoire de Physique Stellaire et Planetaire, France and University of California, U.S.A., collaboration
Proposed	Laboratoire de Physique Stellair et Palnetaire, France and Geneva Observatory, Switzerland collaboration.

First Two Years of IUE' held at the Goddard Space Flight Center, Greenbelt, Maryland, U.S.A.

Besides IUE, various payloads for astronomical observations at UV wavelengths have been launched with rockets and balloons in the last few years or are planned for Shuttle Launched Space Laboratory. Some of these paylaods are listed in Table 6. The wide field UV images of galaxies look particularly promising for studies of star formation in galaxies and could complement IUE observations of elliptical and spiral galaxies.

Acknowledgements

References

Anderson, R. C., Piper, J. G., Broadfoot, A. L. & Wallace, L. (1969) *J. atmos. Sci.* **26**, 874.

Ayres, T. R. & & Linsky, J. (1980) *Ap. J.* **235**, 76.

Baldwin, J. A. (1977) *M.N.R.A.S.* **178**, 67p.

Baldwin, J. A., Rees, M. J., Longair, M. & Peryman, M. A. C. (1978) *Ap. J. (Lett.)* **226**, L57.

Bates, B. *et al.* (1979) *Astr. Ap.* **71**, L22.

Bertola, F., Capaccioli, M., Holm, A. H. & Oke, J. B. (1980) *Ap. J.* **237**, L65.

Black, J. H., Dupree, A. K., Hartmann, L. W. & Raymond, J. C. (1980) *Ap. J.* (in press).

Boggess, A., Wu, C-C., Gondhalekar, P. M. & Wilson, R. (1979) *Proc. First Year of IUE Symp.,* University College, London, p. 182.

Boksenberg, A. (1978) *Phys. Scripta* **17**, 205.

Boksenberg, A. & Sargent, W. L. W. (1978) *Ap. J.* **220**, 42.

Bohlin, R. C., Holm, A. V., Savage, B. D., Snijders, M. A. J. & Sparks, W. M. (1980) *Astr. Ap.* **85**, 1.

Boggess, A. *et al.* (1979) *Ap. J. (Lett.)* **230**, L131.

Borgman, J. (1978) *Astr. Ap.* **69**, 245.

Bromage, G E., Gabrial, A. H. & Sciama, D. W. (1980) *Proc. Second European IUE Conference,* Tubingen, Germany (ESA SP-157) p. 345.

Bromage, G. E., Burton, W. M., Patchett, B. E. & Smith, A. G. (1980) *Proc. Second European IUE Conference,* Tubingen, Germany, (ESA SP-157) p. 267.

Branch, *et al.* (1980) preprint.

Brown, A., Jordan, C. & Wilson, R. (1979) *Proc. First Year of IUE Symp.,* University College London, p. 232.

Burki, G. & de Andrés, F. L. (1979) *Astr. Ap.* **79**, L13.

Chevalier, R. A. & Oegerle, W. R. (1979) *Ap. J.* **227**, 398.

Conti, P. S. & Germany, C. D. (1980) *Ap. J.* **238**, 190.

Code, A. D. & Welch, G. A. (1979) *Ap. J.* **228**, 95.

Cowie, L. L., Jenkins, E. B., Songaila, A. & York, D. C. (1979) *Ap. J.* **232**, 467.

Cram, L. E., Giampapa, M. S. & Imhoff, C. L. (1980) *Ap. J.* **238**, 905.

Darius, J., Giddings, J. R. & Wilson, R. (1979) *Proc. First Year of IUE Symp.,* University College, London, p. 363.

Davidsen, A. F. (1979) *IAU Symp. No. 92.*

de Boer, K. S. & Savage, B. (1980) *Ap. J.* **238**, 86.

de Jager, C., Lamers, H. J. G. L. M., Macchetto, F. & Snow, T. P. (1979) *Astr. Ap.* **79**, L28.

Dupree, A. K., Black, J. H., Davis, R., Hartmann, L. & Raymond, J. C. (1979) *Proc. First Year of IUE Symp.,* University College, London, p. 217.

Dupree, A. K. *et al.* (1980) *Ap. J.* **238**, 969.

Ellis, R. & Gondhalekar P. M. (1980) in preparation.

Ferland, G. T., Rees, M. J., Longair, M. S. & Perryman, M. A. C. (1979) *M.N.R.A.S.* **187**, 65p.

Gondhalekar, P. M., Penston, M. V. & Wilson, R. (1979) *Proc. First Year of IUE Symposium*, University College London, p. 109.

Gondhalekar, P. M. & Wilson, R. (1979) *Proc. First Year of IUE Symposium*, University College London, p. 176.

Gondhalekar, P. M., Carswell, R. F., Morgan, D. H., Nandy, K. & Wilson, R. (1980) *M.N.R.A.S.* in press.

Gondhalekar, P. M., Morgan, D. H., Nandy, K., Wilson, R. (1980) *Proc. Second European IUE Conference*, Tubingen, Germany, (ESA SP-157) p. 131.

Gondhalekar, P.M., Willis, A.J. Morgan, D.H. & Nandy, K. (1980) *M.N.R.A.S.* in press.

Gondhalekar, P. M. & Wilson, R. (1980a) *Nature* **285**, 461.

Gondhalekar, P. M. & Wilson, R. (1980b) in preparation.

Green, *et al.* (1980) *Ap. J.* in press.

Greenfield, E. P., Roberts, D. H. & Burke, B. F. (1980) *Science* **208**, 495.

Greenspan, J. A. & Owen, T. (1967) *Science* **156**, 1489.

Gunn, J. E., Kristian, J., Oke, J. B., Westphal, J. A. & Young, P. J. (1979) *IAU Cir. No. 3431.*

Gursky, H. *et al.* (1980) *Ap. J.* **237**, 163.

Gurzadyan, G. (1975) *Space Sci. Rev.* **18**, 95.

Hammerschlag-Hensberge, G. (1980) *Proc. Second European IUE Conference*, Tubingen, Germany (ESA SP-157) p. lix.

Hartmann, L., Dupree, A. K. & Raymond, J. C. (1980) *Ap. J. (Lett.)* **236**, L143.

Haschik, A. D. & Burke, B. F. (1975). *Ap. J. (Lett.)* **200**, L137.

Hill, J. K. & Bohlin, R. (1980) *Bull. Am. astr. Soc.* 156th Meeting.

Imoff, C. L. & Giampapa, M. S. (1980) *Ap. J. (Lett.)* in press.

Jackson, M. W. *et al.* (1979) *Astr. Ap.* **73**, L7.

Johnson, H. M. (1980) *Ap. J. Lett.* **230**, L137.

Kondo, Y. *et al.* (1980) preprint.

Kupperian, J. E., Milligan, J. E. & Boggess, A. (1958) *Ap. J.* **128**, 453.

Kurt, V. G. & Syunyaev, R. A. (1968) *Soviet Astr.* **11**, 928.

Lebopsky, M. J., Rieke, G. M., Walsh, D. & Weyman, R. J. (1980) *Nature* **285**, 385.

Linsky, J. L. & Haisch, B. M. (1979) *Ap. J.* **229**, L27.

McCray, R. A. (1975) *Proc. Calgary Conference on X-rays in Space*, Calgary, Canada.

McCray, R. A. & Snow, T. P. (1979) *A. Rev. Astr. Ap.* **17**, 213.

Moss, H. W. & Clark, J. T. (1979) *Ap. J. Lett.* **229**, L107.

Morton, D. C. & Spitzer, L. Jr. (1966) *Ap. J.* **144**, 1.

Mullan, D. J. (1976) *Ap. J.* **209**, 171.

Nandy, K., Thompson, G. 1., Jamar, C., Monfils, A. & Wilson, R. (1976) *Astr. Ap.* **51**, 63.

Nandy, K., Morgan, D. H. & Carnochan, D. J. (1979) *M.N.R.A.S.* **186**, 421.

Nandy, K. *et al.* (1980) *Nature* **283**, 752.

Naussbaumer, H. & Schild, H. (1979) *Astr. Ap.* **75**, L17.

O'Connell, R. W. (1976) *Ap. J.* **206**, 370.

Oke, J. B. & Zimmerman, B. A. (1979) *Ap. J. (Lett.)* **231**, L13.

Owen, T. *et al.* (1980) *Ap. J. (Lett.)* **236**, L39.

Panagia, N., *et al.* (1980) *M.N.R.A.S.* in press.

Paschoff, J. M., Linsky, J. L. & Boggess, A. (1979) *Sky and Telescope* **57**, 438.

Peck, M. L. (1980) *Ap. J.* **238**, 79.

Pence, W. (1976) *Ap. J.* **203**, 39.

Pooley, G. G. *et al.* (1979) *Nature* **280**, 461.

Porcas, R. W., Booth, R. S., Browne, I. W. A., Walsh, D. & Wilkinson, P. N. (1979) *Nature* **282**, 385.

Puetter, R. C., Smith, H. E., Soifer, B. T., Willner, S. P. & Pipher, J. L. (1978) *Ap. J. (Lett.)* **226**, L53.

Rahe, J. (1980) *Proc. Second European IUE Conference*, Tubingen, Germany (ESA SP-157) p. xv.

Roberts, D. H., Greenfield, P. E. & Burke, B. F. (1979) *Science* **205**, 894.

Sagan, C. E., Lippincott, E. R., Dayhoff, M. O. & Eck, R. V. (1967) *Nature* **213**, 273.

Sargent, W. L. W. *et al.* (1978) *Ap. J.* **221**, 731.

Savage, B. D. & de Boer, K. S. (1979) *Ap. J. (Lett.)* **230**, L77.

Savage, B. D. & de Boer, K. S. (1980) *Wisconsin Ap. preprint No. 109.*

Sciama, D. W. (1962) *Nature* **204**, 456.

Seaton, M. (1979) *M.N.R.A.S.* **187**, 73p.

Smith, A. M. (1967) *Ap. J.* **147**, 158.

Snijders, M. A. J. (1980) *Proc. Second European IUE Conference,* Tubingen, Germany (ESA SP-157) p. lxxi.

Snijders, M. A. J. *et al.* (1979) *M.N.R.A.S.* **189**, 873.

Snow, J. P. & Morton, D. C. (1976) *Ap. J. Suppl.* **32**, 429.

Spitzer, L. Jr. (1956) *Ap. J.* **124**, 20.

Spitzer, L. Jr. & Jenkins, B. (1975) *A. Rev. Astr. Ap.* **13**, 133.

Stecher, T. P. & Bohlin, R. C. (1980) *Bull. Am. astr. Soc.* 156th Meeting.

Strobel, D. F. (1975) *Rev. Geophys. Sp. Phys.* **13**, 372.

Ulrich, M. H. *et al.* (1980) *M.N.R.A.S.* **192**, 561.

Walsh, D., Carswell, R. F. & Weymann, R. J. (1979) *Nature* **279**, 381.

Weisheit, J. C. & Collins, L. A. (1976) *Ap. J.* **210**, 299.

Weymann, R. J., Chaffee, F H., Davis, M., Carlton, N. P., Walsg, D. & Carswell, R. F. (1979) *Ap. J. (Lett.)* **233**, L43.

Willis, B. J. & Willis, D. (1980) *Ap. J.* **238**, 1.

Young, P. J., Westphal, J. A., Kristian, J., Wilson, C. P. & Landauer, F. P. (1978) *Ap. J.* **221**, 721.

Young, P. J., Gunn, J. E., Kristian, J., Oke, J. B. & Westphal, J. A. (1980) *Ap. J.* in press.